arXiv:1412.4438v1 [cs.CV] 15 Dec 2014

Fixed Point Algorithm Based on Quasi-Newton Method for Convex Minimization Problem with Application to Image Deblurring

Dai-Qiang Chen et.al[*,a,b]

[a]*Department of Mathematics, School of Biomedical Engineering, Third Military Medical University, Chongqing 400038, Chongqing, People's Republic of China*
[b]*Department of Mathematics and System, School of Sciences, National University of Defense Technology, Changsha 410073, Hunan, People's Republic of China*

Abstract

Solving an optimization problem whose objective function is the sum of two convex functions has received considerable interests in the context of image processing recently. In particular, we are interested in the scenario when a non-differentiable convex function such as the total variation (TV) norm is included in the objective function due to many variational models established in image processing have this nature. In this paper, we propose a fast fixed point algorithm based on the quasi-Newton method for solving this class of problem, and apply it in the field of TV-based image deblurring. The novel method is derived from the idea of the quasi-Newton method, and the fixed-point algorithms based on the proximity operator, which were widely investigated very recently. Utilizing the non-expansion property of the proximity operator we further investigate the global convergence of the proposed algorithm. Numerical experiments on image deblurring problem with additive or multiplicative noise are presented to demonstrate that the proposed algorithm is superior to the recently developed fixed-point algorithm in the computational efficiency.

Key words:
Newton method; primal-dual; fixed-point algorithm; total variation; Rayleigh noise

1. Introduction

The general convex optimization problems that arise in image processing take the form of a sum of two convex functions. Often one function is the data fidelity energy term that is decided by the noise type and one wants to minimize, and the other function is the regularization term to make the solution have certain properties. For instance, the usual l_1 based regularization is used to obtain the sparse solution in the fields such as image restoration [1] and compressed sensing [2, 3]. In this paper, we propose an efficient fixed-point algorithm to solve the optimization problem whose objective function is composed of two convex function, i.e.,

$$\min_u f_1(Bu) + f_2(u) \tag{1.1}$$

[*]Corresponding author
Email address: chener050@sina.com (Dai-Qiang Chen et.al)

where $f_1 : \mathbb{R}^M \to \mathbb{R}$ and $f_2 : \mathbb{R}^N \to \mathbb{R}$ are convex function, $B : \mathbb{R}^N \to \mathbb{R}^M$ is a linear transform, and f_2 is differentiable with a $1/\beta$-Lipschitz continuous gradient, i.e.,

$$\langle \nabla f_2(v) - \nabla f_2(w), v - w \rangle \geq \beta \|\nabla f_2(v) - \nabla f_2(w)\|_2^2 \tag{1.2}$$

for any $v, w \in \mathbb{R}^N$. Despite its simplicity, many variational models in image processing can be formulated in the form of (1.1). For example, the classical total variation (TV) or wavelet sparsity prior based models [1], which are often considered in image restoration under Gaussian noise, have the simple form as follows.

$$\min_u \mu \|Bu\|_1 + \frac{1}{2}\|Ku - b\|_2^2 \tag{1.3}$$

where $K \in \mathbb{R}^{N\times N}$ is a linear blurring operator, $b \in \mathbb{R}^N$ and $\mu > 0$ is a regularization parameter. Here B denotes the sparse transform such as the gradient operator and the wavelet basis, and the image prior is imposed by using the term $\|Bu\|_1$, which promotes the sparsity of image under the transform B. With $f_1 = \mu\|\cdot\|_1$ and $f_2 = \frac{1}{2}\|K\cdot - b\|_2^2$ the problem (1.3) can be seen as a special case of (1.1). It is observed that the main difficulty of solving problem (1.1) is that the function f_1 is non-differentiable.

In the last several years, many optimization algorithms have been developed for efficiently solving the variational models in image processing. The iterative shrinkage/thresholding (IST) algorithm is one of the most successful methods. Consider the general minimization problem

$$\min_u f(u) + g(u) \tag{1.4}$$

where f and g are convex function, and g is differentiable. The classical IST algorithm for problem (1.4) is given by the following iterative formula

$$u^{k+1} = \mathcal{T}_{\gamma f}(u^k - \gamma \nabla g(u^k)) = p_\gamma(u^k) \tag{1.5}$$

where $\gamma > 0$ is a step parameter. Here $\mathcal{T}_{\gamma f}$ is called the thresholding operator. It corresponds to the proximity operator $\text{prox}_{\gamma f}$, which is defined by [5]

$$\text{prox}_{\gamma f}(v) = \arg\min_u \gamma f(u) + \frac{1}{2}\|u - v\|_2^2. \tag{1.6}$$

In different literatures, IST is also called iterative denoising method [4], Landweber iteration [6], proximal forward-back splitting (PFBS) algorithm [7] or fixed-point continuation (FPC) algorithm [8]. In order to further accelerate the convergence speed, many new iterative shrinkage algorithms based on the IST, which include the SpaRSA (Sparse Reconstruction by Separable Approximation) [9], TwIST (Two-step IST) [10], FISTA (Fast iterative shrinkage-thresholding algorithm) [11] were further proposed. Notice that a proximity operator is needed to be computed in each iteration of the iterative shrinkage algorithms. However, the proximity operators $\text{prox}_{\gamma f}$ for the general case of $f = f_1 \circ B$ often have no closed solutions. For example, if we choose $B = \nabla$ and $f = \|\nabla \cdot\|_1$, then the minimization problem of (1.6) is just the Rudin-Osher-Fatemi (ROF) denoising problem whose solution cannot be obtained easily. Therefore, inner iterative algorithm is needed for computing the proximity operators in most cases.

In recent years, a class of algorithms based on the splitting methods have been developed and shown to be efficient for computing the proximity operator. For instance, Goldstein and Osher [12] proposed a splitting algorithm based on the Bregman iteration, called the split-Bregman

method, to compute the solution of the minimization problem of (1.6) especially for the case of ROF denoising. This algorithm can be successfully applied for solving the general minimization problem (1.1), and theoretically it has been proved to be equivalent to the Douglas-Rachford splitting (DRS) algorithm [13, 14] and the alternating direction of multiplier method (ADMM) [15, 16]. Although the split-Bregman framework has been shown to be very useful, a sub-minimization problem of solving the system of linear or nonlinear equations is included in each iteration and may time-consuming sometimes. Very recently, alternating direction minimization methods based on the linearized technique [17, 18] have been widely investigated to overcome this and further improve the efficiency. Another class of methods is the primal-dual algorithms. Chambolle [19] firstly proposed a dual algorithm for the ROF denoising. Later on, Zhu et al. [29] devised a primal-dual hybrid gradient (PDHG) method, which alternately update the primal and dual variables by the gradient descent scheme and gradient ascend scheme. The theoretical analysis on variants of the PDHG algorithm, and on the connection with the linearized version or variants of ADMM were widely investigated to bridge the gap between different methods. Refer to [17, 21–24] and the references cited therein for details.

In this paper, we focus our attention on a new class of algorithms that has been developed very recently from the view of fixed-point. In [25], Jia and Zhao proposed a fast algorithm for the ROF denoising by simplify the original split-Bregman framework. Motivated by this idea, Micchelli et al. [26] designed a fixed-point algorithm based on proximity operator (named FP^{2}O) for computing $\text{prox}_{f_1 \circ B}$, which was proved to be more efficient than the splitting methods. Later on, several variants of fixed-point algorithms were proposed for special cases of image restoration. For instance, Micchelli et al. [27, 28] further extended the FP^{2}O algorithm to solve TV-L1 denoising model where $f_2 = \frac{1}{2}\|K \cdot -b\|_1$ in (1.1). Chen et al. [29] proposed a proximity operator based algorithm for solving indicator functions based l_1-norm minimization problems with application to compressed sample. Krol et al. [30] proposed a preconditioned alternating projection algorithm for emission computed tomography (ECT) restoration, where a diagonal preconditioning matrix is used in the devised fixed-point algorithm. The extension of the FP^{2}O algorithm to the more general case of the form of (1.1) has also been investigated very recently [31, 32]. Specifically, a primal-dual fixed point algorithm which combines the PFBS algorithm and only one inner iteration of FP^{2}O has been proposed in [33].

However, in the previous fixed-point algorithms, we observe that all the iterative formulas are composed of the gradient descent algorithm and the proximity point algorithm. It is well known that the gradient-based algorithms typically have a sub-linear convergence rate, while the Newton method or the quasi-Newton method has been presented with a super-linear convergence rate. This fact motivates us to propose a new fixed-point algorithm which combines the quasi-Newton method and the proximity operator algorithm. Furthermore, the global convergence of the proposed algorithm is investigated under certain assumption.

The rest of this paper is organized in four sections. In section 2 we briefly review the existing fixed-point algorithms based on the proximal operator, and further propose a fixed-point algorithm based on quasi-Newton method. In section 3 the global convergence of the proposed algorithm is further investigated from the point of the view of fixed point theory under certain conditions. The numerical examples on deblurring problem of images contaminated by additive Gaussian noise and multiplicative noise are reported in section 4. The results there demonstrate that FP^{2}O$_\kappa$_QN is superior to the recently proposed PDFP^{2}O$_\kappa$ in the context of image deblurring.

2. Fixed-point algorithm based on quasi-Newton method

2.1. Existing fixed-point algorithms based on the proximal operator

Motivated by the fast algorithm proposed for the ROF denoising in the literature [25], Micchelli et al. [26] designed a fixed-point algorithm named FP^{2}O for the computation of the proximity operator $\text{prox}_{f_1\circ B}(x)$ for any $x \in \mathbb{R}^N$. Denote $\lambda_{\max}(BB^T)$ be the largest eigenvalue of BB^T. Choose the parameter $0 < \lambda < 2/\lambda_{\max}$, and define the operator

$$S(v) = \left(I - \text{prox}_{\frac{1}{\lambda}f_1}\right)\left(Bx + \left(I - \lambda BB^T\right)v\right). \tag{2.1}$$

Then we can obtain the fixed-point iterative scheme which is just called FP^{2}O algorithm as follows

$$v^{k+1} = S_\kappa(v^k) \tag{2.2}$$

where S_κ is the κ-averaged operator of S, i.e., $S_\kappa = \kappa I + (1-\kappa)S$ for any $\kappa \in (0,1)$. Calculate the fixed-point v^* of the operator S by the formula (2.2), and hence obtain that

$$\text{prox}_{f_1\circ B}(x) = x - \lambda B^T v^*. \tag{2.3}$$

The key technique served as the foundation of FP^{2}O algorithm is the relationship between the proximity operator and the subdifferential of a convex function, as described in (3.2) below. FP^{2}O algorithm supplies a simple and efficient method of solving (1.1) with the special case of $f_2(u) = \frac{1}{2}\|u - x\|_2^2$ in the classical framework of fixed-point iteration. In [32], this algorithm has been extended to the more general case that $\nabla f_2(u)$ is bijective and the inverse can be computed easily. In particular, choose $f_2(u) = \frac{1}{2}u^T Qu - x^T u$, where Q is a positive definite $N \times N$ matrix. Then (1.1) can be reformulated as

$$\min_u f_1(Bu) + \frac{1}{2}u^T Qu - x^T u \tag{2.4}$$

Define the operator

$$\hat{S}(v) = \left(I - \text{prox}_{\frac{1}{\lambda}f_1}\right)\left(BQ^{-1}x + \left(I - \lambda BQ^{-1}B^T\right)v\right). \tag{2.5}$$

Then the corresponding fixed-point iterative scheme for (2.4) is given by

$$v^{k+1} = \hat{S}_\kappa(v^k), \tag{2.6}$$

and the solution u^* of (2.4) can be obtained by the formula

$$u^* = Q^{-1}\left(x - \lambda B^T v^*\right) \tag{2.7}$$

where v^* is the fixed-point of the operator $\hat{S}_\kappa$.

In order to deal with the general case of f_2, the authors in [31] also combined FP^{2}O and PFBS algorithms, and proposed a new algorithm named PFBS_FP^{2}O in which the proximity operator in the PFBS algorithm is calculated by using FP^{2}O, i.e.,

$$u^{k+1} = \text{prox}_{\gamma f_1\circ B}\left(u^k - \gamma\nabla f_2(u^k)\right)$$

is calculated by FP^{2}O. Notice that a inner iteration of solving $\text{prox}_{\gamma f_1 \circ B}$ is included in PFBS_FP^{2}O, and it is problematic to set the approximate iteration number to balance the computational time and precision. In order to solve this issue, a primal-dual fixed points algorithm based on proximity operator (PDFP^{2}O) [33] was proposed very recently. In this algorithm, instead of implementing FP^{2}O for many iteration steps to calculate $\text{prox}_{\gamma f_1 \circ B}(x)$ in PFBS_FP^{2}O, only one inner fixed-point iteration is adopted. Suppose $\kappa = 0$. Then we can obtain the following iteration scheme (PDFP^{2}O):

$$\begin{cases} u^{k+1/2} = u^k - \gamma \nabla f_2(u^k), \\ v^{k+1} = \left(I - \text{prox}_{\frac{\gamma}{\lambda} f_1}\right)\left(Bu^{k+1/2} + \left(I - \lambda BB^T\right)v^k\right), \\ u^{k+1} = u^{k+1/2} - \lambda B^T v^{k+1}. \end{cases} \tag{2.8}$$

It is obvious that u is the primal variable related to (1.1), and according to the thorough study in [33] we know that the variable v is just the dual variable of the primal-dual form related to (1.1). Therefore, PDFP^{2}O also belongs to the class of primal-dual algorithm framework. Similarly to FP^{2}O, a relaxation parameter $\kappa \in (0, 1)$ can be introduced to get the algorithm named PDFP^{2}O$_\kappa$. For more details refer to [33].

2.2. Proposed fixed-point algorithm based on quasi-Newton method

In the PDFP^{2}O algorithm, the iterative formulas consist of the proximity operator and the gradient descent algorithm. Since the Newton-type methods have been shown to have a faster convergence rate compared to the gradient-based methods, a very nature idea is to use the Newton-type methods instead of the gradient descent step in the fixed-point algorithm. Consider the minimization problem (1.1). We use the second-order Taylor expansion of the convex function $f_2(u)$ at the recent iterative point u^k instead of it, i.e.,

$$f_2(u) \approx f_2(u^k) + \langle \nabla f_2(u^k), u - u^k \rangle + \frac{1}{2}\left(u - u^k\right)^T Q^k \left(u - u^k\right)$$

where Q^k is a positive definite symmetric matrix to approximate the second derivative $\nabla^2 f_2$. Then (1.1) can be reformulated as

$$\min_u f_1(Bu) + \frac{1}{2}u^T Q^k u - (Q^k u^k - \nabla f_2(u^k))^T u. \tag{2.9}$$

It is observed that (2.9) corresponds to the minimization problem (2.4) with $x = Q^k u^k - \nabla f_2(u^k)$. Therefore, the next iteration scheme u^{k+1} can be obtained by the fixed point iteration algorithm shown in (2.5)–(2.7). In order to avoid any inner iterations, we use only one inner fixed point iteration in the proposed algorithm. For this, choose $\kappa = 0$, and define

$$S_{k+1}(v) = \left(I - \text{prox}_{\frac{1}{\lambda} f_1}\right)\left(B(u^k - (Q^k)^{-1}\nabla f_2(u^k)) + \left(I - \lambda B(Q^k)^{-1}B^T\right)v\right).$$

Using the numerical solution v^k for S_k as the initial value, and only implementing one iteration of solving the fixed-point of $S_{k+1}(v)$, we can obtain the following iteration scheme

$$\begin{cases} v^{k+1} = \left(I - \text{prox}_{\frac{1}{\lambda} f_1}\right)\left(B(u^k - (Q^k)^{-1}\nabla f_2(u^k)) + \left(I - \lambda B(Q^k)^{-1}B^T\right)v^k\right), \\ u^{k+1} = u^k - (Q^k)^{-1}\nabla f_2(u^k) - \lambda(Q^k)^{-1}B^T v^{k+1}. \end{cases} \tag{2.10}$$

Setting $u^{k+1/2} = u^k - (Q^k)^{-1}\nabla f_2(u^k)$. It is observed that an intermediate iterative variable $u^{k+1/2}$ is generated by a quasi-Newton method. Therefore, we called the proposed algorithm a fixed-point algorithm based on quasi-Newton method, and abbreviate it as FP^{2}O_QN, which is described as **Algorithm 1** below. For simplification of convergence analysis below, we set $Q^k \equiv Q$ to be unchanged with different k.

Algorithm 1 Fixed-point algorithm based on quasi-Newton method (FP^{2}O_QN)

Initialization: set $u_0 \in \mathbb{R}^N$, $v_0 \in \mathbb{R}^M$, $0 < \lambda \leq 1/\lambda_{\max}(BQ^{-1}B^T)$.

Main Iteration:

$u^{k+1/2} = u^k - Q^{-1}\nabla f_2(u^k)$;

$v^{k+1} = \left(I - \text{prox}_{\frac{1}{\lambda}f_1}\right)\left(Bu^{k+1/2} + \left(I - \lambda BQ^{-1}B^T\right)v^k\right)$;

$u^{k+1} = u^{k+1/2} - \lambda Q^{-1}B^T v^{k+1}$.

Similarly to the literatures [26, 32, 33], we can introduce a relaxation parameter $\kappa \in (0, 1]$ to obtain **Algorithm 2**, which is exactly the Picard iterates with the parameter.

Algorithm 2 FP^{2}O$_\kappa$_QN

Initialization: set $u_0 \in \mathbb{R}^N$, $v_0 \in \mathbb{R}^M$, $0 < \lambda \leq 1/\lambda_{\max}(BQ^{-1}B^T)$.

Main Iteration:

$u^{k+1/2} = u^k - Q^{-1}\nabla f_2(u^k)$;

$\hat{v}^{k+1} = S_{k+1}(v^k)$;

$\hat{u}^{k+1} = u^{k+1/2} - \lambda Q^{-1}B^T v^{k+1}$.

$v^{k+1} = \kappa v^k + (1-\kappa)\hat{v}^{k+1}$;

$u^{k+1} = \kappa u^k + (1-\kappa)\hat{u}^{k+1}$.

3. Convergence analysis

Let us start with some related notations and conclusions which will serve as the foundation for the proof below.

Definition 3.1. *(Nonexpansive operator) A nonlinear operator $T : \mathbb{R}^M \to \mathbb{R}^M$ is called nonexpansive if for any $x, y \in \mathbb{R}^M$,*

$$\|T(x) - T(y)\|_2 \leq \|x - y\|_2.$$

A nonlinear operator $P : \mathbb{R}^M \to \mathbb{R}^M$ is called firmly nonexpansive if for any $x, y \in \mathbb{R}^M$,

$$\|P(x) - P(y)\|_2^2 \leq \langle x - y, Px - Py\rangle.$$

By the application of the Cauchy-Schwarz inequality it is easy to show that a firmly nonexpansive operator is also nonexpansive.

Definition 3.2. *(Picard sequence [34])For a given initial point $v^0 \in \mathbb{R}^M$ and an operator $P : \mathbb{R}^M \to \mathbb{R}^M$, the sequence $\{v^k : k \in \mathbb{N}\}$ generated by $v^{k+1} = P(v^k)$ is called the Picard sequence of the operator P.*

For the Picard sequence we have the following conclusion.

Proposition 3.3. *(Opial κ-averaged Theorem [34]) Let C be a closed convex set in $\mathbb{R}^M$ and let $P : C \to C$ be a nonexpansive mapping with at least one fixed point. Then for any $v^0 \in R^M$ and any $\kappa \in (0, 1)$, the Picard sequence of $P_\kappa = \kappa I + (1 - \kappa)P$ converges to a fixed point of P.*

For any convex function $f : \mathbb{R}^N \to \mathbb{R} \bigcup \{+\infty\}$, the subdifferential of f at $x \in \mathbb{R}^N$ is defined by

$$\partial f(x) = \left\{ y \in \mathbb{R}^N : f(z) \geq f(x) + \langle y, z - x \rangle, \ \ \forall\, z \in \mathbb{R}^N \right\}. \tag{3.1}$$

The following result illustrates the relationship between the proximity operator and the subdifferential of a convex function. This conclusion has appeared in many previous literatures, such as [26, 32, 33].

Proposition 3.4. *If f is a convex function defined on $\mathbb{R}^N$ and $x, y \in \mathbb{R}^N$, then*

$$y \in \partial f(x) \Leftrightarrow x = prox_f(x + y). \tag{3.2}$$

In what follows, we establish a fixed-point formulation for the solution of the minimization problem (1.1) based on the conclusion in Proposition 3.4. To this end, we define the operator $T_1 : \mathbb{R}^M \times \mathbb{R}^N \to \mathbb{R}^M$ as

$$T_1(v, u) = \left(I - \text{prox}_{\frac{1}{\lambda} f_1}\right)\left(B(u - Q^{-1}\nabla f_2(u)) + \left(I - \lambda B Q^{-1} B^T\right) v\right), \tag{3.3}$$

and the operator $T_2 : \mathbb{R}^M \times \mathbb{R}^N \to \mathbb{R}^N$ as

$$T_2(v, u) = u - Q^{-1}\nabla f_2(u) - \lambda Q^{-1} B^T T_1 \tag{3.4}$$

where λ is a positive parameter. Denote the operator $T : \mathbb{R}^M \times \mathbb{R}^N \to \mathbb{R}^M \times \mathbb{R}^N$ as

$$T(v, u) = (T_1(v, u), T_2(v, u)). \tag{3.5}$$

Theorem 3.5. *If u^* is a solution of the minimization problem (1.1), then there exists $v^* \in R^M$ that satisfies:*

$$v^* = T_1(v^*, u^*), \quad u^* = T_2(v^*, u^*)$$

which implies that (v^*, u^*) is a fixed point of T. Conversely, if $w^* = (v^*, u^*)$ is a fixed point of T, then u^* is a solution of the minimization problem (1.1).

Proof: Since u^* is one solution of the minimization problem (1.1), by the first-order optimality condition we have

$$\begin{aligned} & 0 \in \nabla f_2(u^*) + (B^T \circ \partial f_1 \circ B)(u^*) \\ \Leftrightarrow\ & 0 \in Q^{-1}\nabla f_2(u^*) + (Q^{-1}B^T \circ \partial f_1 \circ B)(u^*) \\ \Leftrightarrow\ & u^* \in u^* - Q^{-1}\nabla f_2(u^*) - \lambda\left(Q^{-1}B^T \circ \frac{1}{\lambda}\partial f_1 \circ B\right)(u^*). \end{aligned}$$

Denote $v^* = \left(\frac{1}{\lambda}\partial f_1 \circ B\right)(u^*)$. Then we obtain that

$$u^* = u^* - Q^{-1}\nabla f_2(u^*) - \lambda Q^{-1} B^T v^*. \tag{3.6}$$

Besides, using Proposition 3.4 we have

$$\begin{aligned} v^* = \left(\frac{1}{\lambda}\partial f_1 \circ B\right)(u^*) &\Leftrightarrow Bu^* = \operatorname{prox}_{\frac{1}{\lambda}f_1}(Bu^* + v^*) \\ &\Leftrightarrow v^* = \left(I - \operatorname{prox}_{\frac{1}{\lambda}f_1}\right)(Bu^* + v^*). \end{aligned} \tag{3.7}$$

Inserting (3.6) into (3.7) we further obtain that

$$v^* = \left(I - \operatorname{prox}_{\frac{1}{\lambda}f_1}\right)(B(u^* - Q^{-1}\nabla f_2(u^*)) + (I - \lambda BQ^{-1}B^T)v^*). \tag{3.8}$$

Based on (3.6) and (3.8) we infer that (v^*, u^*) is a fixed point of T.

Conversely, if there exists $w^* = (v^*, u^*)$ satisfying $w^* = T(w^*)$, we can derive that u^* satisfies the first-order optimality condition of (1.1) by the equivalent formulas above. Therefore, we conclude that u^* is a solution of (1.1). □

According to the formulas in (3.3) and (3.4) we find out that the iterative scheme of FP^{2}O_QN can be reformulated as

$$\begin{cases} v^{k+1} = T_1(v^k, u^k), \\ u^{k+1} = T_2(v^k, u^k) \end{cases}$$

which is also equal to $w^{k+1} = T(w^k)$ with $w^k = (v^k, u^k)$. This implies that the sequence $\{v^k, u^k\}$ generated by FP^{2}O_QN is just the Picard sequence of the operator T. With the similar discussion we can find that the iterative formulas of FP^{2}O$_\kappa$_QN is equal to $w^{k+1} = T\kappa(w^k)$, i.e., the sequence $\{v^k, u^k\}$ generated by FP^{2}O$_\kappa$_QN is the Picard sequence of the operator T_κ.

Based on Theorem 3.5 we know that the solution of the minimization problem (1.1) is just equal to the fixed point of the operator T. Therefore, the convergence of FP^{2}O$_\kappa$_QN can be guaranteed by verifying the nonexpansion of T according to Proposition 3.3. The proof here is similar to those presented in [33]. However, note that the global convergence of proposed algorithms cannot be directly obtained by applying results in [33], and hence it is included here for completion.

In the following, we give a crucial inequality for showing the nonexpansion of T. Denote

$$h(u) = u - Q^{-1}\nabla f_2(u),$$

$$M = I - \lambda BQ^{-1}B^T.$$

Here we assume that $0 < \lambda \leq 1/\lambda_{\max}(BQ^{-1}B^T)$, and hence M is a symmetric positive semi-definite matrix. Therefore, we can define the semi-norm $\|u\|_M = \sqrt{u^T M u}$, and then define the norm

$$\|w\|_{\lambda,Q} = \sqrt{\|u\|_Q^2 + \lambda\|v\|_2^2}.$$

Lemma 3.6. *For any two points $w_1 = (v_1, u_1)$ and $w_2 = (v_2, u_2)$ in $\mathbb{R}^M \times \mathbb{R}^N$, the following inequality*

$$\begin{aligned} \|T(w_1) - T(w_2)\|_{\lambda,Q}^2 \leq \|w_1 - w_2\|_{\lambda,Q}^2 &- \|\nabla f_2(u_1) - \nabla f_2(u_2)\|_{2\beta - Q^{-1}}^2 \\ &- \|v_1 - v_2\|_{I-M}^2 - \lambda\|T_1(w_1) - T_1(w_2) - (v_1 - v_2)\|_M^2 \end{aligned} \tag{3.9}$$

comes into existence.

Proof: According to Lemma 2.4 of [7] we know that $I - prox_{\frac{1}{\lambda}f}$ is firmly nonexpansive, and hence obtain

$$\begin{aligned}\|T_1(w_1) - T_1(w_2)\|_2^2 &\le \langle T_1(w_1) - T_1(w_2), B(h(u_1) - h(u_2)) + M(v_1 - v_2)\rangle \\ &= \langle T_1(w_1) - T_1(w_2), B(h(u_1) - h(u_2))\rangle + \langle T_1(w_1) - T_1(w_2), M(v_1 - v_2)\rangle.\end{aligned} \tag{3.10}$$

Following the definition in (3.4) we also have

$$\begin{aligned}&\|T_2(w_1) - T_2(w_2)\|_Q^2 \\ &= \|h(u_1) - h(u_2) - \lambda Q^{-1}B^T(T_1(w_1) - T_1(w_2))\|_Q^2 \\ &= \|h(u_1) - h(u_2)\|_Q^2 - 2\lambda\langle h(u_1) - h(u_2), B^T(T_1(w_1) - T_1(w_2))\rangle \\ &+ \lambda\|T_1(w_1) - T_1(w_2)\|_2^2 - \lambda\|T_1(w_1) - T_1(w_2)\|_M^2.\end{aligned} \tag{3.11}$$

According to (3.10) and (3.11) we further have

$$\begin{aligned}&\|T(w_1) - T(w_2)\|_{\lambda,Q}^2 \\ &= \|T_2(w_1) - T_2(w_2)\|_Q^2 + \lambda\|T_1(w_1) - T_1(w_2)\|_2^2 \\ &= \|h(u_1) - h(u_2)\|_Q^2 - \lambda\|T_1(w_1) - T_1(w_2)\|_M^2 \\ &+ 2\lambda\|T_1(w_1) - T_1(w_2)\|_2^2 - 2\lambda\langle h(u_1) - h(u_2), B^T(T_1(w_1) - T_1(w_2))\rangle \\ &\le \|h(u_1) - h(u_2)\|_Q^2 - \lambda\|T_1(w_1) - T_1(w_2)\|_M^2 + 2\lambda\langle T_1(w_1) - T_1(w_2), M(v_1 - v_2)\rangle \\ &= \|h(u_1) - h(u_2)\|_Q^2 + \lambda\|v_1 - v_2\|_M^2 - \lambda\|T_1(w_1) - T_1(w_2) - (v_1 - v_2)\|_M^2.\end{aligned} \tag{3.12}$$

Since f_2 has $1/\beta$-Lipschitz continuous gradient, we get that

$$\begin{aligned}&\|h(u_1) - h(u_2)\|_Q^2 \\ &= \|u_1 - u_2\|_Q^2 - 2\langle\nabla f_2(u_1) - \nabla f_2(u_2), u_1 - u_2\rangle + \|\nabla f_2(u_1) - \nabla f_2(u_2)\|_{Q^{-1}}^2 \\ &\le \|u_1 - u_2\|_Q^2 - \|\nabla f_2(u_1) - \nabla f_2(u_2)\|_{2\beta - Q^{-1}}^2.\end{aligned} \tag{3.13}$$

By the definition of M we easily get

$$\|v_1 - v_2\|_M^2 = \|v_1 - v_2\|_2^2 - \|v_1 - v_2\|_{I-M}^2. \tag{3.14}$$

Based on (3.12)–(3.14) we can obtain (3.9) directly. □

From the results in Lemma 3.6 we know that T is nonexpansive with the norm of $\|\cdot\|_{\lambda,Q}$. Therefore, we are able to prove the convergence of FP^{2}O$_\kappa$-QN according to Proposition 3.3, which is described as follows.

Theorem 3.7. *Assume that $\|Q^{-1}\|_2 < 2\beta$ and $0 < \lambda \le 1/\lambda_{\max}(BQ^{-1}B^T)$. Let (v^k, u^k) be the sequence generated by FP^{2}O$_\kappa$-QN. Then (v^k, u^k) converges to the fixed point of T and u^k converges to the solution of (1.1).*

Proof: Note that the solution of (1.1) is just one fixed point of T. From Lemma 3.6 we know that the operator T is nonexpansive, maps the set $\mathbb{R}^M \times \mathbb{R}^N$ to itself, and has at least one fixed point. According to Opial κ-averaged Theorem, we conclude that, for any w^0 and $\kappa \in (0,1)$, the Picard sequence of T_κ converges to a fixed point of T. With this result we further infer that u^k converges to the solution of (1.1). □

Finally, we process with the convergence of FP^{2}O_QN based on the inequality in Lemma 3.6.

Theorem 3.8. *Assume that* $\|Q^{-1}\|_2 < 2\beta$ *and* $0 < \lambda \leq 1/\lambda_{\max}(BQ^{-1}B^T)$. *Let* (v^k, u^k) *be the sequence generated by FP*^{2}*O_QN. Then* (v^k, u^k) *converges to the fixed point of* T *and* u^k *converges to the solution of (1.1).*

Proof: Let $w^* = (v^*, u^*) \in \mathbb{R}^M \times \mathbb{R}^N$ be a fixed point of T. Substitute w_1 and w_2 in (3.9) with $w^k = (v^k, u^k)$ and w^*, we obtain that

$$\|w^{k+1} - w^*\|^2_{\lambda,Q} \leq \|w^k - w^*\|^2_{\lambda,Q} - \|\nabla f_2(u^k) - \nabla f_2(u^*)\|^2_{2\beta - Q^{-1}} - \|v^k - v^*\|^2_{I-M} - \lambda\|v^{k+1} - v^k\|^2_M. \quad (3.15)$$

Summing (3.15) from some k_0 to $+\infty$ we obtain that

$$\sum_{k=k_0}^{+\infty} \left\{ \|\nabla f_2(u^k) - \nabla f_2(u^*)\|^2_{2\beta - Q^{-1}} + \|v^k - v^*\|^2_{I-M} + \lambda\|v^{k+1} - v^k\|^2_M \right\} \leq \|w^{k_0} - w^*\|^2_{\lambda,Q} \quad (3.16)$$

which implies that

$$\lim_{k\to+\infty} \|\nabla f_2(u^k) - \nabla f_2(u^*)\|^2_{2\beta - Q^{-1}} = 0, \quad (3.17)$$

$$\lim_{k\to+\infty} \|v^k - v^*\|^2_{I-M} = 0, \quad (3.18)$$

$$\lim_{k\to+\infty} \|v^{k+1} - v^k\|^2_M = 0. \quad (3.19)$$

According to (3.18) we can easily deduce that $\lim_{k\to+\infty} \|v^{k+1} - v^k\|^2_{I-M} = 0$, and combining it with (3.19) we have

$$\lim_{k\to+\infty} \|v^{k+1} - v^k\|^2_2 = 0. \quad (3.20)$$

Besides, from (3.6) we know that $Q^{-1}\nabla f_2(u^*) + \lambda Q^{-1}B^T v^* = 0$, and hence obtain that

$$u^{k+1} - u^k = -Q^{-1}(\nabla f_2(u^k) - \nabla f_2(u^*)) - \lambda Q^{-1}B^T(v^{k+1} - v^*). \quad (3.21)$$

Based on (3.21) we immediately get

$$\begin{aligned} \|u^{k+1} - u^k\|^2_Q &\leq \|Q^{-1}(\nabla f_2(u^k) - \nabla f_2(u^*))\|^2_Q + \|\lambda Q^{-1}B^T(v^{k+1} - v^*)\|^2_Q \\ &= \|(\nabla f_2(u^k) - \nabla f_2(u^*))\|^2_{Q^{-1}} + \lambda\|v^{k+1} - v^*\|^2_{I-M}. \end{aligned} \quad (3.22)$$

Since $0 < \|Q^{-1}\|_2 < 2\beta$, utilizing (3.17) and (3.18) we can deduce from (3.22) that

$$\lim_{k\to+\infty} \|u^{k+1} - u^k\|_Q^2 = 0. \tag{3.23}$$

Combining (3.20) and (3.23) we further obtain that

$$\lim_{k\to+\infty} \|w^{k+1} - w^k\|_{\lambda,Q} = 0. \tag{3.24}$$

According to (3.15) we know that the sequence $\left\{\|w^k - w^*\|_{\lambda,Q}^2\right\}$ is non-increasing, and hence $\left\{w^k\right\}$ is bounded, which implies that there exists a convergent subsequence of $\left\{w^{k_j}\right\}$ such that

$$\lim_{j\to+\infty} \|w^{k_j} - \hat{w}^*\|_{\lambda,Q} = 0 \tag{3.25}$$

for some point $\hat{w}^* = (\hat{v}^*, \hat{u}^*)$. Due to the operator T is continuous, we further have $\lim_{j\to+\infty} \|T(w^{k_j}) - T(\hat{w}^*)\|_{\lambda,Q} = 0$. Besides, we have

$$\|T(w^{k_j}) - \hat{w}^*\|_{\lambda,Q} \le \|w^{k_j+1} - w^{k_j}\|_{\lambda,Q} + \|w^{k_j} - \hat{w}^*\|_{\lambda,Q} \tag{3.26}$$

which implies that

$$\lim_{j\to+\infty} \|T(w^{k_j}) - \hat{w}^*\|_{\lambda,Q} = 0 \tag{3.27}$$

based on (3.24) and (3.25). Therefore, $\hat{w}^*$ is a fixed point of the operator T. Due to the proof is started with any fixed point w^*, we can set $w^* = \hat{w}^*$. In this case, we see that the sequence $\left\{\|w^k - \hat{w}^*\|_{\lambda,Q}\right\}$ is non-increasing. Combining this with the formula (3.25) we infer that

$$\lim_{k\to+\infty} w^k = \hat{w}^*. \tag{3.28}$$

From Theorem 3.5 we know that $\hat{u}^*$ is a solution of (1.1). This completes the proof. □

4. Numerical examples

In this section, we will compare the proposed FP^{2}O$_\kappa$_QN algorithm with PDFP^{2}O$_\kappa$ [33] through the experiments of image restoration. Here two cases of additive and multiplicative noise types are considered. One is the additive Gaussian noise which has been extensively investigated over the last decades. In this setting, the data fidelity term can be formulated as

$$f_2(u) = \frac{1}{2}\|Ku - b\|_2^2$$

where K is the blurring operator, and b is the observed image. The other is the speckle noise which also appears in many real world image processing applications such as laser imaging, synthetic aperture radar (SAR) imaging and ultrasonic imaging. In [35], this speckle noise followed by a Rayleigh distribution is investigated. Under this condition, the observed image can be modeled as corrupted with signal-dependent noise of this form

$$b = Ku + \sqrt{Ku}\varepsilon \tag{4.1}$$

where ε is a zero-mean Gaussian noise with standard deviation σ, i.e., $\varepsilon \sim N(0, \sigma)$. Based on the model (4.1) and the characteristics of Gaussian distribution, the corresponding fidelity term can be formulated as

$$f_2(u) = \sum_i \frac{(b - Ku)_i^2}{(Ku)_i}.$$

In the following experiments, we use total variation as the regularization term, and hence choose the function

$$f_1(Bu) = \mu \|\nabla u\|_1$$

where $\nabla : \mathbb{R}^N \to \mathbb{R}^{2N}$ is a discrete gradient operator. Here we adopt the isotropic definition of total variation, and the proximity operator $\text{prox}_{\frac{1}{\lambda} f_1}$ can be computed easily. For more details refer to [32].

4.1. Gaussian image deblurring

In this subsection, we choose three gray-scale images, Cameraman, Barbara (with size of 256×256), and Boat (with size of 512×512) as the original images, and evaluate FP^{2}O$_\kappa$_QN in four typical image blurring scenarios: strong blur with low noise; strong blur with medium noise; mild blur with low noise; mild blur with medium noise, which are summarized in Table 1 (σ and σ_a denote the standard deviation).

Table 1: Description of image blurring scenarios

Scenario	Blur kernel	Gaussian noise
1	8×8 box average kernel	$\sigma = 1.5$
2	8×8 box average kernel	$\sigma = 3$
3	6×6 gaussian kernel with $\sigma_a = 8$	$\sigma = 1.5$
4	6×6 gaussian kernel with $\sigma_a = 8$	$\sigma = 3$

In the following, we discuss the selection of the parameters μ, λ and κ in both fixed point algorithms, the parameter γ in PDFP^{2}O$_\kappa$, and the matrix Q in FP^{2}O$_\kappa$_QN. Due to $f_2(u) = \frac{1}{2}\|Ku - b\|_2^2$, we have $\nabla^2 f_2 \equiv K^T K$. Therefore, we can choose $Q = K^T K$. However, the blurring operator K is ill-posed generally, and $(K^T K)^{-1}$ cannot be used in the proposed algorithm due to the instability. Therefore, we choose $Q = K^T K + \epsilon B^T B$ in our experiments. Here ϵ is a small positive number and B is a difference matrix. Notice that the introduction of the term $\epsilon B^T B$ avoids the ill-posed condition, and Q^{-1} can also be computed efficiently by fast Fourier transforms (FFTs) with periodic boundary conditions.

The regularization parameter μ is decided by the noise level, and the adjustment of the parameters λ and γ does influence the convergence speed and stability of the fixed point algorithms. Through many trials we use the rules of thumb: μ is set to 0.06 and 0.15 for $\sigma = 1.5$ and 3.0 respectively; λ is set to 0.125; γ is chosen to be 1.8 for PDFP^{2}O$_\kappa$; and $\epsilon = 0.1$ for FP^{2}O$_\kappa$_QN. Similarly to the literatures [32, 33], we find that $\kappa = 0$ achieves the best convergence speed compared with other $\kappa \in (0, 1)$, and hence we choose $\kappa = 0$ for both algorithms.

The performance of the restored images of the compared algorithms is measured quantitatively by means of the peak signal-to-noise ratio (PSNR), which is defined by

$$\text{PSNR}(u, \overline{u}) = 10 \lg \left\{ \frac{255^2 N}{\|u - u^*\|_2^2} \right\} \tag{4.2}$$

where u and u^* denote the original image and the restored image respectively. The stopping criterion for the fixed-point algorithms is defined such that the relative error is below some small constant, i.e.,

$$\frac{\|u^{k+1} - u^k\|_2}{\|u^k\|_2} < tol \tag{4.3}$$

where tol denotes a prescribed tolerance value. In our experiments we choose $tol = 5 \times 10^{-4}$.

The PSNR values for the deblurred images, the number of iterations, and the CPU time are listed in Table 2. In this table, the four image blurring scenarios shown in Table 1 are considered, and $(\cdot, \cdot, \cdot)$ represents the PSNR values, iteration numbers and CPU time in sequence. From these results we observe that the recovered images obtained by FP^{2}O$_\kappa$_QN can achieve better PSNRs than those given by PDFP^{2}O$_\kappa$, and meanwhile, the corresponding iteration number and running time of FP^{2}O$_\kappa$_QN is less than those of PDFP^{2}O$_\kappa$. Figures 1–3 show the recovery results of the PDFP^{2}O$_\kappa$ and FP^{2}O$_\kappa$_QN algorithms. It is observed that the visual qualities of images obtained by both algorithms are more or less the same.

Table 2: The comparison of the performance of both fixed point algorithms: the given numbers are PSNR (dB)/Iteration number/CPU time(second)

Scenario	1	2	3	4
Image	Cameraman			
PDFP^{2}O$_\kappa$	(26.16, 97, 1.87)	(25.63, 102, 2.04)	(27.58, 89, 1.67)	(26.74, 88, 1.59)
FP^{2}O$_\kappa$_QN	(26.75, 46, 1.06)	(25.91, 42, 0.81)	(28.02, 45, 0.97)	(26.98, 42, 0.84)
Image	Barbara			
PDFP^{2}O$_\kappa$	(25.11, 73, 1.42)	(24.35, 74, 1.49)	(27.90, 75, 1.44)	(26.60, 75, 1.45)
FP^{2}O$_\kappa$_QN	(25.29, 38, 0.78)	(24.40, 34, 0.72)	(28.06, 39, 0.75)	(26.65, 38, 0.74)
Image	Boat			
PDFP^{2}O$_\kappa$	(28.64, 73, 5.27)	(27.83, 78, 6.09)	(30.11, 65, 4.98)	(28.95, 69, 5.19)
FP^{2}O$_\kappa$_QN	(29.35, 34, 3.57)	(28.15, 32, 3.31)	(30.64, 33, 3.28)	(29.20, 32, 3.24)

Figure 4 shows the evolution curves of PSNR values obtained by both fixed point algorithms for two cases including in Table 2: one is the Cameraman image blurred by 8×8 box average kernel and added with Gaussain noise with $\sigma = 3$, the other is the Boat image blurred by 6×6 gaussian kernel and added with Gaussain noise with $\sigma = 1.5$. From the plots we can implicitly find that FP^{2}O$_\kappa$_QN achieves the best solution (with higher PSNRs) much faster than PDFP^{2}O$_\kappa$.

4.2. Rayleigh image deblurring

In this subsection, we further discuss the case of images contaminated by Rayleigh noise. The corresponding minimization problem has been introduced above. The two blur kernels shown in Table 1, and Rayleigh noise with $\sigma = 0.5$ and 1.0 are considered here.

First of all, we illustrate the setting of the parameters in both fixed point algorithms. Since $f_2(u) = \sum_i \frac{(b-Ku)_i^2}{(Ku)_i}$, we have that

$$\nabla^2 f_2(\xi) = 2K^T \left(\frac{b^2}{(K\xi)^3} \right) K$$

for any $\xi \in \mathbb{R}^N$. Notice that the value of $\nabla^2 f_2$ changes with the iteration number, and the inverse of $\nabla^2 f_2$ is difficult to be estimated. Therefore, we use $Q = \beta K^T K + \epsilon$ to approximate $\nabla^2 f_2$ in

(a) (b)

(c) (d)

Figure 1: (a) The original Cameraman image, (b) the blurry and noisy image in the scenario 2, PSNR=20.96dB, (c) the image restored by PDFP^{2}O$_\kappa$, (d) the image restored by FP^{2}O$_\kappa$_QN.

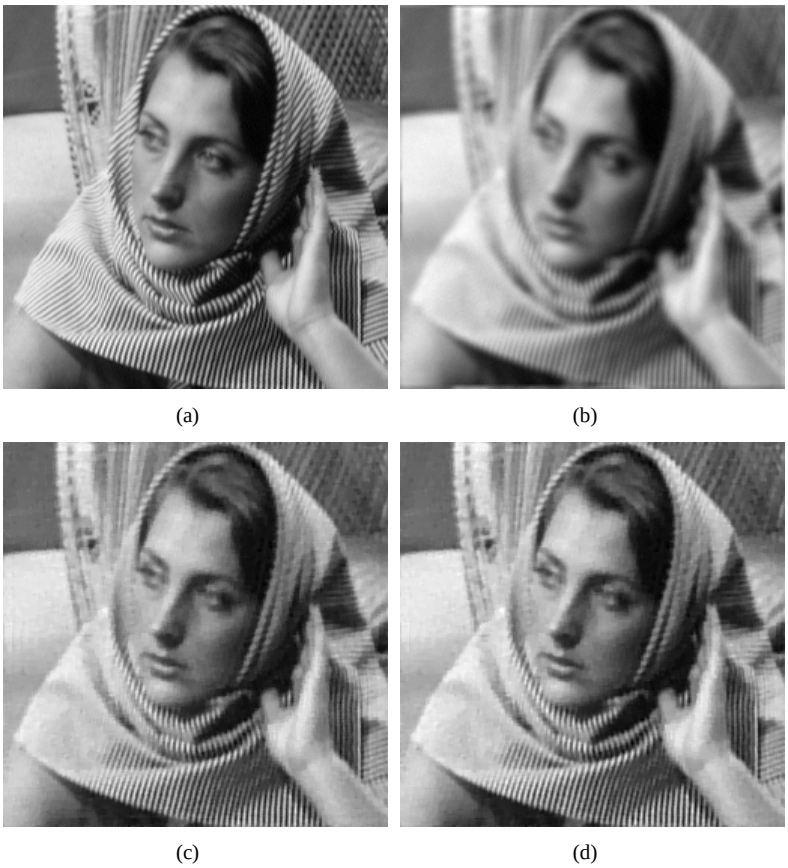

(a) (b)

(c) (d)

Figure 2: (a) The original Barbara image, (b) the blurry and noisy image in the scenario 3, PSNR=22.62dB, (c) the image restored by PDFP^{2}O$_\kappa$, (d) the image restored by FP^{2}O$_\kappa$_QN.

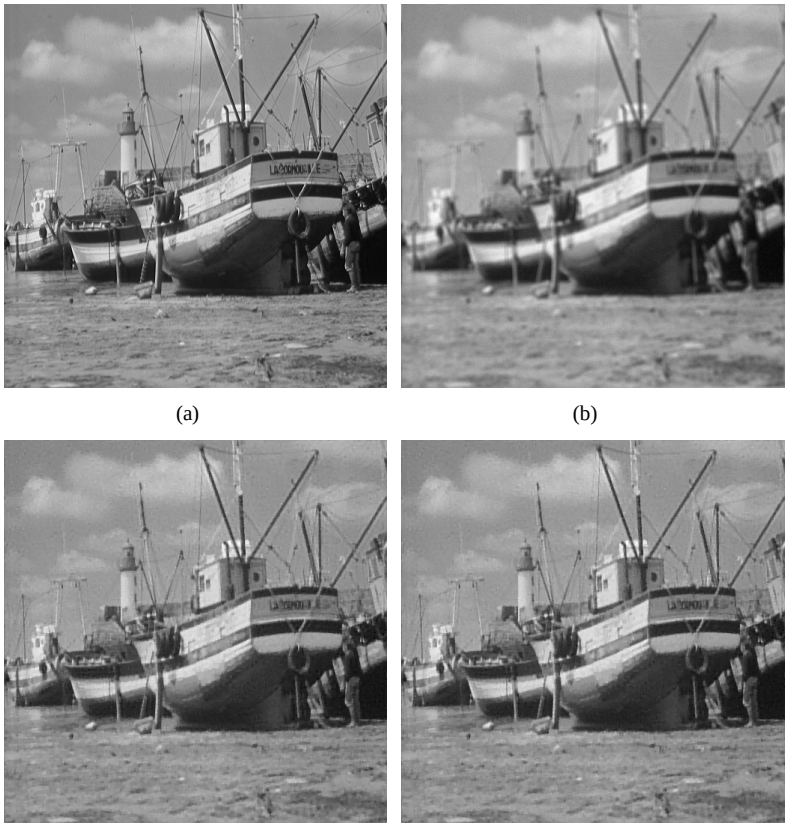

(a) (b)

(c) (d)

Figure 3: (a) The original Boat image, (b) the blurry and noisy image in the scenario 4, PSNR=24.74dB, (c) the image restored by PDFP^{2}O$_\kappa$, (d) the image restored by FP^{2}O$_\kappa$_QN.

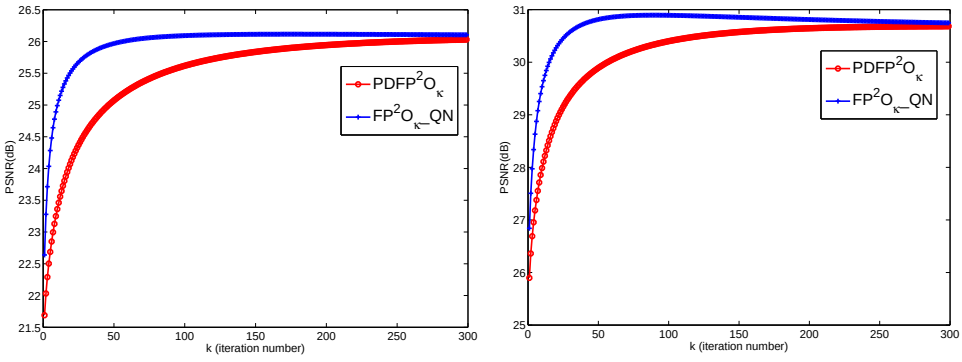

(a) (b)

Figure 4: The evolution curves of PSNR (dB) for images with different blur kernels and noise levels. (a) Cameraman image in the scenario 2; (b) Boat image in the scenario 3.

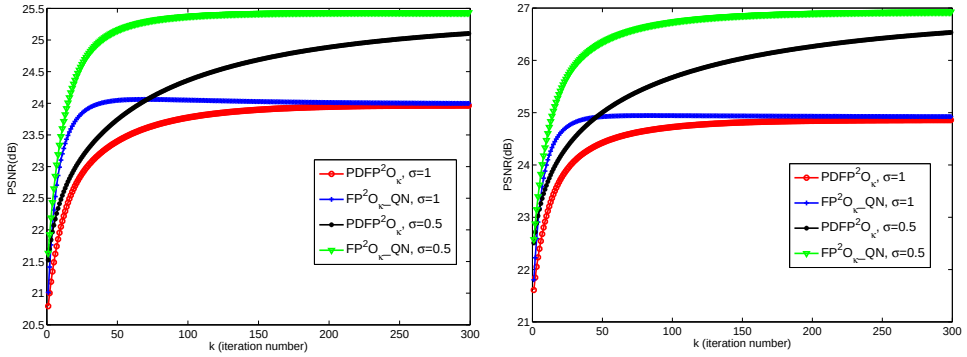

(a) (b)

Figure 5: The evolution curves of PSNR (dB) for Pepper image with different blur kernels and noise levels. (a) Pepper image blurred by 8×8 box average kernel; (b) Pepper image blurred by 6×6 gaussian kernel.

the proposed fixed point algorithm. Here the parameter β is used to replace the unknown $\frac{b^2}{(K\xi)^3}$, and the term $\epsilon B^T B$ is included to avoid the ill-posed condition. In the following experiments, we find that $\beta = 0.25$ and $\epsilon = 0.005$ are two suitable selection through many trials. Moreover, for parameters in both algorithms we use the following rules of thumb: the regularization parameter μ is chosen to be 0.01 and 0.02 for the noise level of $\sigma = 0.5$ and 1.0 respectively; λ is set to 0.125; γ is chosen to be 15.0 for PDFP^{2}O$_\kappa$. We also find out that the selection of $\kappa = 0$ is suitable for our experiments here.

In what follows, two images, Pepper (with size of 256×256) and Cameraman, are used for our test. Figures 5–6 show the evolution curves of PSNR (dB) running both fixed point algorithms for the two images. From the plots we observe that the PSNR values obtained by FP^{2}O$_\kappa$_QN increase much faster than those by PDFP^{2}O$_\kappa$. This is due to the quasi-Newton method included in FP^{2}O$_\kappa$_QN is more efficient than the gradient descent algorithm involved in PDFP^{2}O$_\kappa$.

Figure 7 shows the deblurred results of Pepper image convoluted by 8×8 box average kernel and contaminated by Rayleigh noise with $\sigma = 1.0$. The corresponding PSNR values, the number of iterations, and the CPU time are also included. It is observed that FP^{2}O$_\kappa$_QN can obtain higher PSNR values with less iteration number and running time compared to PDFP^{2}O$_\kappa$. The recovery results of Cameraman image blurred by 6×6 gaussian kernel and corrupted by Rayleigh noise with $\sigma = 1.0$ are also presented in Figure 8. We also observe that FP^{2}O$_\kappa$_QN is more efficient than PDFP^{2}O$_\kappa$, especially in the implementation time.

5. Conclusion

In this article, we propose a fast fixed point algorithm based on the quasi-Newton method, abbreviated as FP^{2}O$_\kappa$_QN, for solving the minimization problems with the general form of $\min_{u \in \mathbb{R}^N} \{f_1(Bu) + f_2(u)\}$. The main distinction between FP^{2}O$_\kappa$_QN and previous fixed point algorithms lies in that the quasi-Newton method, rather than the gradient descent algorithm, is included in the algorithm framework. The proposed algorithm framework is applied to solve TV-based image restoration problem. Numerical experiments reported in this paper indicate that FP^{2}O$_\kappa$_QN outperform the recently proposed PDFP^{2}O$_\kappa$, especially in the implementation time.

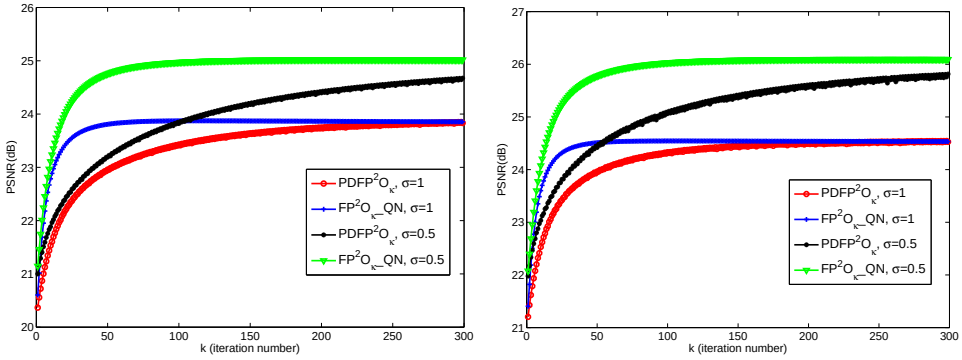

(a) (b)

Figure 6: The evolution curves of PSNR (dB) for Cameraman image with different blur kernels and noise levels. (a) Cameraman image blurred by 8×8 box average kernel; (b) Cameraman image blurred by 6×6 gaussian kernel.

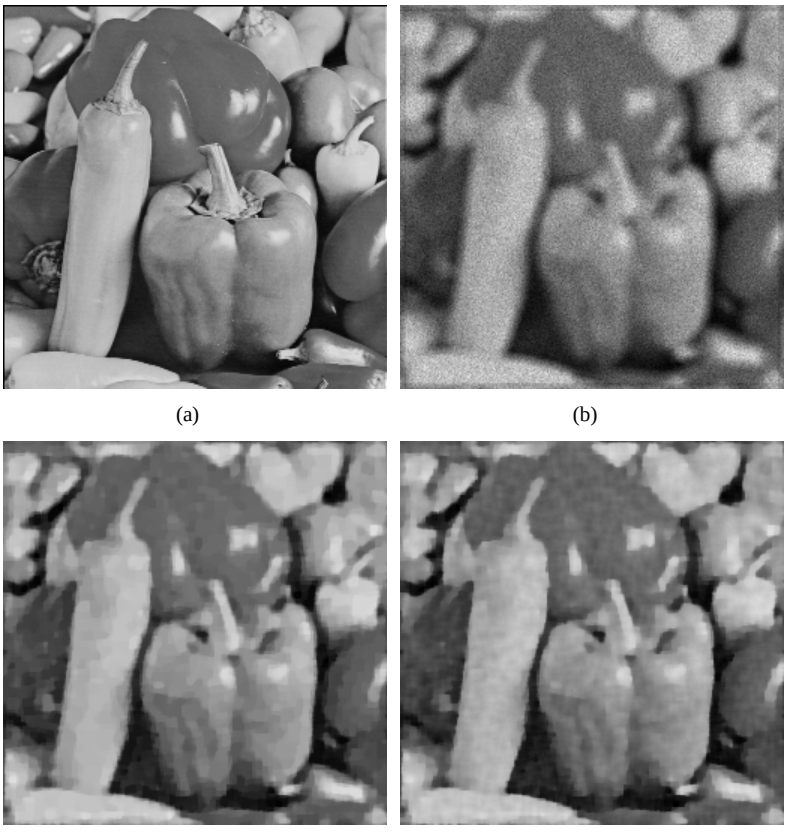

(a) (b)

(c) (d)

Figure 7: (a) The original Pepper image, (b) the blurry and noisy image, (c) the image restored by PDFP^{2}O$_\kappa$, PSNR=23.83, iter.=115, time=2.29, (d) the image restored by FP^{2}O$_\kappa$_QN, PSNR=24.04, iter.=48, time=1.40.

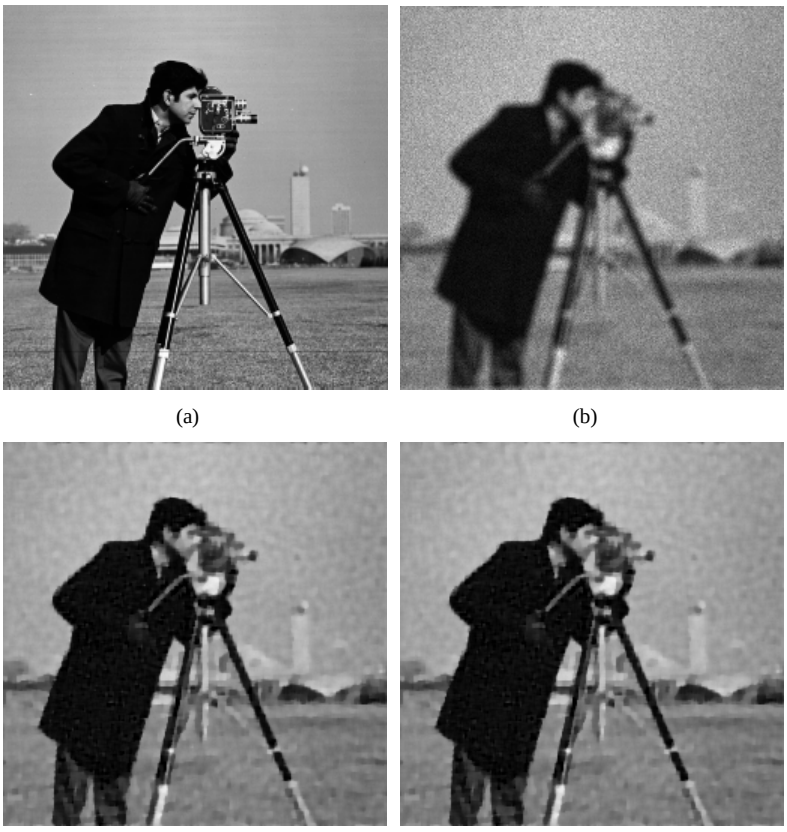

(a) (b)

(c) (d)

Figure 8: (a) The original Cameraman image, (b) the blurry and noisy image, (c) the image restored by PDFP^{2}O$_\kappa$, PSNR=24.36, iter.=108, time=2.24, (d) the image restored by FP^{2}O$_\kappa$_QN, PSNR=24.49, iter.=45, time=1.14.

6. Acknowledgments

The research was supported in part by the National Natural Science Foundation of China under Grant 61271014.

References

[1] S. Ma, W. Yin, Y. Zhang, and A. Chakraborty, An efficient algorithm for compressed MR imaging using total variation and wavelets, IEEE International Conference on Computer Vision and Pattern Recognition (CVPR) 2008, (2008).

[2] E. J. Candès, J. Romberg, and T. Tao, Robust uncertainty principles: Exact signal reconstruction from highly incomplete frequency information, IEEE Transactions on Information Theory, 52 (2006), pp. 489-509.

[3] D. Donoho, Compressed sensing, IEEE Transactions on Information Theory, 52 (2006), pp. 1289-1306.

[4] Figueiredo M, Nowak R. An EM algorithm for wavelet-based image restoration. IEEE Trans. Image Process., 2003, 12: 906-916.

[5] J. J. Moreau: Proximité et dualité dans un espace hilbertien. Bulletin de la Societé Mathématique de France 93,273-299(1965)

[6] Daubechies I, Defrise M, Mol C D. An iterative thresholding algorithm for linear inverse problems with a sparsity constraint. Commun. Pure Appl. Math., 2004, 57: 1413-1457.

[7] Combettes P, Wajs V. Signal recovery by proximal forward-backward splitting. SIAM Multiscale Model. Simul, 2005, 4: 1168-1200.

[8] Hale E, Yin W, Zhang Y. A fixed-point continuation method for l1-regularized minimization with applications to compressed sensing. Rice University: Department of Computational and Applied Mathematics, 2007.

[9] Wright S, Nowak R, Figueiredo M. Sparse reconstruction by separable approximation. IEEE Trans. Signal Process., 2009, 57(7):2479-2493.

[10] Dias J B, Figueiredo M. A new TwIST: two-step iterative shrinkage/thresholding algorithms for image restoration. IEEE Trans. Image Process., 2007, 16(12):2992-3004.

[11] Beck A, Teboulle M. A fast iterative shrinkage-thresholding algorithm for linear inverse problems. SIAM J. Imaging Sci., 2009, 2(1):183-202.

[12] Goldstein T, Osher S. The Split Bregman Method for L1 Regularized Problems. SIAM J. Imaging Sci., 2009, 2(2):323-343.

[13] P. L. Combettes and J. C. Pesquet: A Douglas-Rachford splitting approach to nonsmooth convex variational signal recovery. IEEE J. Selected Topics in Signal Processing 1, 564-574(2007)

[14] Setzer S. Operator Splittings, Bregman Methods and Frame Shrinkage in Image Processing. Int. J. Comput. Vis., 2011, 92(3):265-280

[15] Esser E. Applications of Lagrangian-based alternating direction methods and connections to split Bregman. UCLA: Department of Mathematics, 2009.

[16] D. Chen, L. Cheng and F. Su: A new TV-Stokes model with augmented Lagrangian method for image denoising and deconvolution. J. Sci. Comput. 51(3), 505-526 (2012)

[17] D. Q. Chen and Y. Zhou, Multiplicative Denoising Based on Linearized Alternating Direction Method Using Discrepancy Function Constraint, J. Sci. Comput., (2013), doi: 10.1007/s10915-013-9803-z.

[18] D. Q. Chen, Regularized Generalized Inverse Accelerating Linearized Alternating Minimization Algorithm for Frame-Based Poissonian Image Deblurring, SIAM J. Imag. Sci., 7(2) (2014), pp. 716-739.

[19] A. Chambolle, An algorithm for total variation minimization and applications, Special issue on mathematics and image analysis. J. Math. Imaging Vis., 20 (2004), 89-97.

[20] M. Zhu and T. Chan, An Efficient Primal-Dual Hybrid Gradient Algorithm for Total Variation Image Restoration, Technical Report 08-34, CAM UCLA, 2008.

[21] Chambolle A, Pock T. A first-order primal-dual algorithm for convex problems with applications to imaging. J. Math. Imaging Vis., 2011, 40(1): 120-145.

[22] Pock, T., and Chambolle, A. (2011, November). Diagonal preconditioning for first order primal-dual algorithms in convex optimization. In Computer Vision (ICCV), 2011 IEEE International Conference on (pp. 1762-1769). IEEE.

[23] Esser E, Zhang X, Chan T F. A general framework for a class of first order primal-dual algorithms for convex optimization in imaging science. SIAM Journal on Imaging Sciences, 2010, 3(4): 1015-1046.

[24] He B, Yuan X. Convergence analysis of primal-dual algorithms for a saddle-point problem: From contraction perspective. SIAM Journal on Imaging Sciences, 2012, 5(1): 119-149.

[25] R. Q. Jia and H. Zhao: A fast algorithm for the total variation model of image denoising. Adv. Comput. Math. 33, 231-241(2010)

[26] C. A. Micchelli, L. X. Shen, and Y. S. Xu: Proximity Algorithms for Image Models: Denoising. Inverse Problems, 27 (2011)
[27] Micchelli, C. A., Shen, L., Xu, Y., and Zeng, X. Proximity algorithms for the L1/TV image denoising model. Adv. Comput. Math., 38(2), 401-426 (2013).
[28] Chen, F., Shen, L., Xu, Y., and Zeng, X. (2014). The Moreau Envelope Approach for the L1/TV Image Denoising Model. Inverse Problems and Imaging, 8(1), 53-77.
[29] Chen, F., Shen, L., Suter, B. W., and Xu, Y. A Proximity Algorithm Solving Indicator Functions Based l1-Norm Minimization Problems in Compressive Sampling., Technical Report 12-63, CAM UCLA, 2012.
[30] Krol, A., Li, S., Shen, L., and Xu, Y. Preconditioned alternating projection algorithms for maximum a posteriori ECT reconstruction. Inverse problems, 28(11), 115005 (2012).
[31] Argyriou A, Micchelli C A, Pontil M, Shen L and Xu Y, Efficient first order methods for linear composite regularizers Arxiv preprint arXiv:1104.1436 (2011).
[32] D. Q. Chen, H. Zhang, L. Z. Cheng, A Fast Fixed Point Algorithm for Total Variation Deblurring and Segmentation, J. Math. Imaging Vis., 43(3), 167-179 (2012).
[33] Chen, P., Huang, J., and Zhang, X. (2013). A primal-dual fixed point algorithm for convex separable minimization with applications to image restoration. Inverse Problems, 29(2), 025011.
[34] Z. Opial: Weak convergence of the suquence of successive approximations for nonexpansive mappings. Bulletin American Mathematical Society 73, 591-597(1967)
[35] Krissian, K., Kikinis, R., Westin, C.F., Vosburgh, K.: Speckle constrained filtering of ultrasound images. IEEE Comput. Vis. Pattern Recogn. 547-552 (2005)